

Pseudo[n,m]rotaxanes of Cucurbit[7/8]uril and Viologen-Naphthalene Derivative: A Precise Definition of Rotaxane

Beilin Zhang,^{a,†} Yunhong Dong,^{a,b,‡} Jie Li,^a Yang Yu,^a Chenyang Li,^a and Liping Cao^{*a}

^a Key Laboratory of Synthetic and Natural Functional Molecule Chemistry of the Ministry of Education, College of Chemistry and Materials Science, Northwest University, Xi'an, Shaanxi 710069, China

^b National Demonstration Center for Experimental Chemistry Education, College of Chemistry and Materials Science, Northwest University, Xi'an, Shaanxi 710069, China

Cite this paper: *Chin. J. Chem.* 2019, 37, 269–275. DOI: 10.1002/cjoc.201800562

Summary of main observation and conclusion Rotaxane is a kind of classic supramolecule, which is usually constructed from a number of macrocycles and one axis molecule. Herein, we have expanded the supramolecular structure of [n]rotaxane to offer a precise definition of (pseudo)[n,m]rotaxane for accurately describing the two kinds of (pseudo)rotaxanes structures, which are self-assembled from cucurbit[7/8]uril (CB[7/8]) and viologen-naphthalene derivative, respectively. Furthermore, these CB-based pseudorotaxanes exhibit varied photophysical properties, stimuli-responsive behavior triggered by competitive guest, and self-sorting behavior.

Background and Originality Content

In recent decades, mechanically interlocked molecules (MIMs) have received considerable attention as molecular machines (*e.g.* molecular switches,^[1] molecular motors^[2] and molecular catalysts^[3]), which can be defined as a kind of functional supramolecular structure formed from a number of discrete molecular units through non-covalent interactions. For examples, rotaxanes, catenanes,^[4] and knots, as classic MIMs, have been widely studied due to not only their fascinating supramolecular architectures but also their potential applications.^[5] One of the most popular MIMs is rotaxane, defined by Schill in 1971.^[6] Usually, it contains one or several cyclic molecules (roda) and a linear molecule (axis). The linear and cyclic molecules are held by supramolecular interactions "mechanical-bonding" rather than by covalent or coordinate bonds. To prevent cyclic molecules from sliding out of linear molecule, two groups of sufficiently large size are applied to the stopper at both ends of the molecule. If the linear molecule can be removed from the inner cavity of the cyclic molecules, the supramolecule formed by cyclic and linear molecules is called pseudorotaxane.

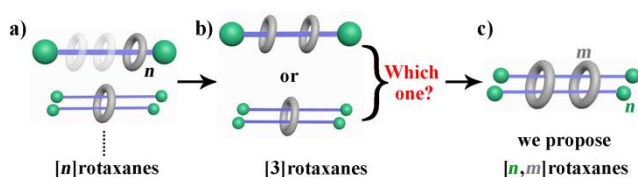
In previous reports, people often use [n]rotaxane to represent different structures of rotaxanes, where ' n ' represents the number of assembled molecules, containing both cyclic and linear molecules. However, the assembled structures of rotaxanes are becoming diversity, which results in that a simple ' n ' cannot accurately represent a complicated assembled structure (Scheme 1a). For example, [3]rotaxane, referring to two possible assembled modes: 1) one linear molecule and two macrocycles; 2) two linear ones and one macrocycle (Scheme 1b). Herein, we have expanded

the supramolecular structures of [n]rotaxane to offer a precise definition of (pseudo)[n,m]rotaxanes, where ' n ' represents the number of axis molecules and ' m ' represents the number of macrocyclic molecule, for accurately describing the assembled structures of (pseudo)rotaxanes (Scheme 1c).

The cucurbit[n]uril family ($n = 5-8, 10$) formed from cyclic methylene-bridged glycoluril oligomers possess a hydrophobic cavity and two cyclic carbonyl portals.^[7] They can bind various organic molecules through hydrophobic interaction and van der Waals interactions of the cavity or hydrogen bond and ion-dipole interactions of carbonyl groups at two cyclic portals.^[8] As a result, cucurbit[n]uril can choose guest molecules with an appropriate size to form inclusion complexes, and then assemble into MIM structures. In the cucurbit[n]uril family, cucurbit[7]uril (CB[7]) has a cavity with the portal diameter of 5.4 Å and an inner diameter is 7.3 Å, which can encapsulate one aromatic guest to form binary complex.^[9] Compared with CB[7], cucurbit[8]uril (CB[8]) has a larger cavity, with the portal diameter of 6.9 Å and an inner diameter is 8.8 Å, which can form ternary complexes by encapsulating two identical (*e.g.*, diphenylpyridinium^[10]) or different (*e.g.*, naphthalene units and the viologen segments^[11,12]) guest molecules. Therefore, CB[7/8] are suitable building blocks for constructing various (pseudo)rotaxane.

Recently, supramolecular chemists have used CB[n] as a macrocyclic host to synthesize many disperse rotaxanes or infinite polyrotaxanes through their unique host-guest properties. For example, one-dimensional (pseudo)rotaxanes based on CB[n] from 1 : 1 or 1 : 2 stoichiometry,^[13] two-dimensional network (pseudo)rotaxanes (*e.g.*, polyrotaxane,^[14] molecular necklace^[15]), and extended three-dimensional (pseudo)rotaxanes,^[16] have been constructed to exhibit applications in cell imaging,^[17] supramolecular organic framework,^[18] white-light emissions,^[19] and so on. Specifically, CB[8]-based pseudorotaxanes have exhibited a discrete structure of novel 2 : 2 model system of host-guest inclusions.^[20] For example, Scherman and co-workers studied CB[8]-diarylvologen host-guest complexes and verified them to be 2 : 2 quaternary complexes rather than previously reported 1 : 1 binary complexes.^[21] In this paper, we obtained two kinds of 1 : 2 and 2 : 2 CB-based pseudorotaxanes formed from CB[7/8] and viologen-

Scheme 1 Cartoon illustrations of propose definition of [n,m]rotaxanes



*E-mail: chcaoliping@nwu.edu.cn. ‡These authors contributed equally.

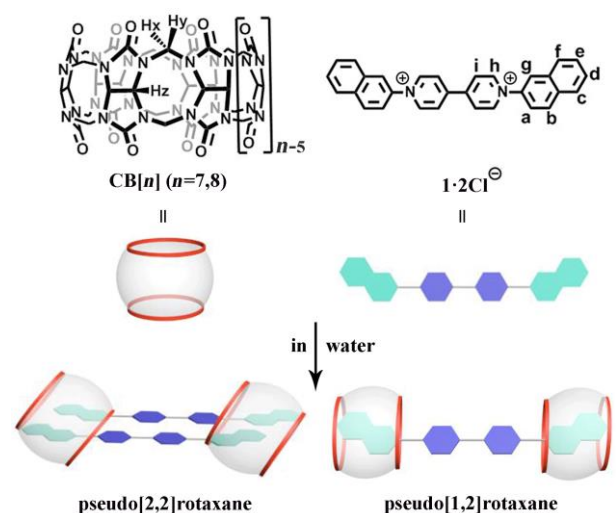
†Dedicated to the Special Issue of "Supramolecular Chemistry".

For submission: <https://mc.manuscriptcentral.com/cjoc>

For articles: <https://onlinelibrary.wiley.com/journal/16147065>

naphthalene derivative (**1**), respectively. According to our precise definition for rotaxane, 2+2 quaternary complex between viologen-naphthalene derivative and CB[8] can be represented as pseudo[2,2]rotaxane rather than just pseudo[4]rotaxane, and 1+2 ternary complex between viologen-naphthalene derivative and CB[7] can be represented as pseudo[1,2]rotaxane rather than just pseudo[3]rotaxane (Scheme 2). Following this way, complicated (pseudo)rotaxanes can be named easily.

Scheme 2 Schematic illustration of pseudo[2,2]rotaxane $1_2 \cdot \text{CB}[8]_2$ and pseudo[1,2]rotaxane $1 \cdot \text{CB}[7]_2$



Results and Discussion

Viologen derivatives as their cationic property and suitable size are suitable recognition units of guests for fabricating host-guest complex with cucurbit[*n*]uril.^[21,22] Therefore, we designed and synthesized a linear and water-soluble guest, 2,2'-dinaphthalene-4,4'-bipyridine-1,1'-dium dichloride (**1**), containing a viologen unit in the middle and two naphthalene ring units at both terminals. Guest **1** was synthesized by the Zincke reaction of 2-naphthylamine with *N,N'*-bis(2,4-dinitrophenyl) 4,4'-bipyridine-1,1'-dium chloride salt, in 89% yield.

Fortunately, we obtained brown needle-like single crystals of **1** from MeOH solution by slow vapor diffusion of iPr₂O at room temperature. Figure 1 illustrates the single molecule and stacking structures of **1**. The dihedral angle of two pyridine rings units in the center of **1** is about 37.4°, while the dihedral angle of the two naphthalene rings at two terminals is about 24.5°. And the dihedral angles of two pyridine ring and their adjacent naphthalene rings are about 31.6° and 33.4°, respectively. Subsequently, as shown in Figure 1b, the adjacent molecules with each other are arranged in a parallel and partially overlapped pattern of stacking along *c* axis in stacking layers. Between the layers, both of the adjacent naphthalene rings, naphthalene ring and the viologen ring are stacked by $\pi \cdots \pi$ interactions ($d = \sim 3.48$ Å). The front view of stacking structure **1**·**1** is alternate permutation from the *c* axis in Figure 1c. Furthermore, the adjacent layers of **1** are connected with each other by the solvent molecules and anions to form a 3D structure through weak non-covalent interactions (Figure S3).

Based on the different size of CB[7/8]'s cavities, CB[7] can just bind one molecule, while CB[8] with a large cavity can encapsulate two liner molecules simultaneously to form a multiaxial (pseudo)rotaxane. Therefore, we presumed that viologen-naphthalene derivative **1** would be self-assembled with CB[7/8] to generate two kinds of pseudorotaxanes by the host-guest interaction with different stoichiometric ratios. Initially, we used NMR and ITC technology to research the self-assembly behavior between **1** and

CB[7/8]. ¹H NMR titration experiments were performed by adding 0–2.0 equiv. of **1** to a solution of CB[8] (0.5 mmol/L) in D₂O (Figure 2). When 0–1.0 equiv. of **1** was added to a solution of CB[8] (0.5 mmol/L), the signals of free **1** disappeared completely and only one new set of resonances showed up, indicating the formation of supramolecular assembly with 1 : 1 binding stoichiometry (Figure 2a–d). All the proton signals of the naphthalene ring were fully assigned based on a ¹H–¹H COSY experiment (Figures S4). Compared with the peaks of free **1**, we found that there were obvious upfield shift ($\Delta\delta = \sim 1.0$) of the protons (H_{a-g}) on the naphthalene ring, which indicated that CB[8] bound with the naphthalene ring moiety at two terminals rather than the viologen moiety in the middle of the guest. And one of the viologen protons ($H_{i'}$) exhibited slight upfield shift by approximately δ 0.04, suggesting an inclusion near the portal of CB[8] and average signals deriving from a partial inclusion and partial exclusion by the cavity; another viologen proton ($H_{i'}$) shifted downfield slightly by approximately δ 0.09, suggesting a location near the carbonyl portal yet outside the CB[*n*] cavity. Compared with free CB[8], all the resonance

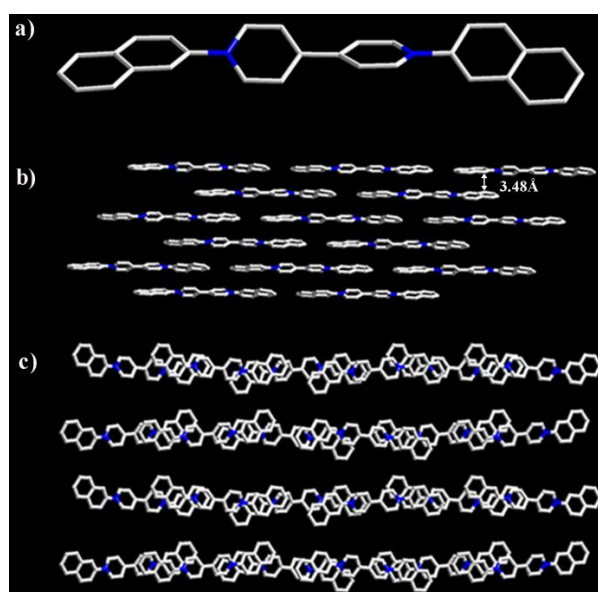


Figure 1 The single-crystal X-ray structures of (a) a single molecule of **1**; (b) side view of stacking structure **1**·**1** from the *b* axis and (c) front view of stacking structure **1**·**1** from the *c* axis. Color code: C, grey; N, blue. Hydrogen atoms and chloride ions to balance the charge have been omitted for clarity.

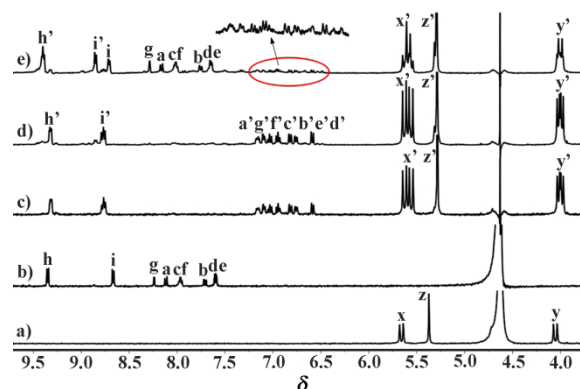


Figure 2 ¹H NMR spectra recorded (400 MHz, 298 K, D₂O) for: (a) CB[8] (0.5 mmol/L), (b) **1** (0.5 mmol/L), (c) CB[8] (0.5 mmol/L) and **1** (0.5 equiv.), (d) CB[8] (0.5 mmol/L) and **1** (1.0 equiv.), (e) CB[8] (0.5 mmol/L) and **1** (2.0 equiv.). Here, primes (') denote resonances within the host-guest complexes.

peaks of bound CB[8] shifted upfield slightly (δ 0.05–0.08) (Figure 2d). Moreover, the signals of free **1** could be observed by adding 2.0 equiv. of **1** (Figure 2e), indicating a slow exchange between bound and unbound **1** on the NMR time scale. Furthermore, when more **1** existed, the protons (H_h) of viologen exhibited slight downfield shift by approximately δ 0.08 and another proton (H_i) split into two signals. The DOSY experiment was performed to explain the change of these protons. In Figure S5, two sets of different diffusion coefficients of $(1.758 \pm 0.144) \times 10^{-10} \text{ m}^2 \cdot \text{s}^{-1}$ and $(3.522 \pm 0.100) \times 10^{-10} \text{ m}^2 \cdot \text{s}^{-1}$ were observed, respectively. It indicates the existence of two species of different sizes, so we concluded that the split signals (H_i) belonged to free and complexed **1**, the average proton (H_h) signals derived from partial inclusion and partial free in Figure 2e.

The stoichiometry of the complex between **1** and CB[8] is 1 : 1 ratio as well as the isothermal titration calorimetry (ITC) (Figure 3a). The ITC curves fitted well to a 1 : 1 binding model with a high binding constant of $K_a = (1.06 \pm 0.33) \times 10^7 \text{ L} \cdot \text{mol}^{-1}$, suggesting that the strong binding facilitates the stable self-assemblies in water. However, in the present case of $(\mathbf{1} \cdot \text{CB}[8])_n$, the binding stoichiometry is clearly 2 : 2 rather than 1 : 1, confirmed through the electrospray ionization mass spectrometry (ESI-MS), NOESY NMR, and 2D diffusion ordered spectroscopy (DOSY) (Figures 3, 4, S6). In the ESI-MS spectrum, not only 1 + 1 complex of CB[8] and **1** but also 2 + 2 were observed, which confirmed that a quaternary complex, pseudo[2,2]rotaxane ($\mathbf{1}_2 \cdot \text{CB}[8]_2$) may exist. NOESY NMR was employed to further confirm our quaternary binding model and to investigate the stacking model of the two **1** molecules within the cavity of CB[8] (Figure 3b). In NOESY spectrum, there were H_g - H_e and H_b - H_d inter-correlation between two naphthalene rings, suggesting that one benzene ring of naphthalene moiety in the complex should indeed be close to the benzene ring from another naphthalene moiety, and two complexed **1** molecules likely stack with each other in a partially overlapped pattern rather than directly stacking of each other. As a result, each CB[8] molecule includes two naphthalene groups from the neighboring two guest molecules with a face-to-face arrangement, and the inclusion mode is a 2 : 2 binding motif to form pseudo[2,2]rotaxane. Meanwhile, DOSY further confirmed the formation of a single species in the solution with diffusion coefficient of $(1.571 \pm 0.065) \times 10^{-10} \text{ m}^2 \cdot \text{s}^{-1}$, which is much lower than that of 1 : 1 complex (Figure 4a).

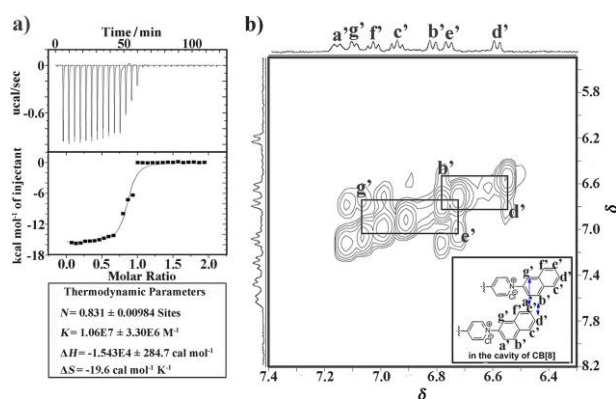


Figure 3 (a) ITC data for the titration of CB[8] (20 $\mu\text{mol/L}$) in the cell with a solution of **1** (180 $\mu\text{mol/L}$) in the syringe in H_2O at 298 K. (b) NOESY NMR spectrum recorded (400 MHz, D_2O , 298 K, 1 mmol/L) of $\mathbf{1}_2 \cdot \text{CB}[8]_2$.

Similarly, ^1H NMR titration experiment was also performed to research the host-guest interaction between **1** and CB[7] (Figure S7). There were significant changes of the protons on naphthalene, which were attributed to the shielding effect exerted by the cavity of CB[7]. All the proton signals of the naphthalene ring were fully assigned based on a ^1H - ^1H COSY experiment (Figure S8). Under

the addition of over 2.0 equiv. of CB[7] into **1**, the resonances did not further shift, indicating that the stoichiometry of the complex between **1** and CB[7] is 1 : 2 ratio (Figure S7). ITC curves fitted well to a 1 : 2 binding model with $n = 0.58$ with binding constants $K = (3.74 \pm 0.72) \times 10^6 \text{ L} \cdot \text{mol}^{-1}$ (Figure S9). In addition, we only found 1 + 1 complex of CB[7] and **1** through the electrospray ionization mass spectrometry (ESI-MS), which suggested that pseudo[1,2]-rotaxane ($\mathbf{1} \cdot \text{CB}[7]_2$) may be unstable under the condition of ESI-MS (Figure S10). By comparing two sets of diffusion coefficients of $\mathbf{1}_2 \cdot \text{CB}[8]_2$ and $\mathbf{1} \cdot \text{CB}[7]_2$, we found diffusion coefficient of $\mathbf{1}_2 \cdot \text{CB}[8]_2$ is smaller than that of $\mathbf{1} \cdot \text{CB}[7]_2$ (Figure 4b), which confirmed $\mathbf{1}_2 \cdot \text{CB}[8]_2$ possessed more larger self-assembled systems with 2 + 2 mode. Furthermore, Job's plot by using UV-vis spectroscopy displays a maximum absorption change at 0.3 and 0.5 (Figures S11 and S12), which confirmed that the stoichiometry of the complex between **1** and CB[7/8] is 1 : 2 for pseudo[1,2]rotaxane ($\mathbf{1} \cdot \text{CB}[7]_2$) and 2 : 2 for pseudo[2,2]rotaxane ($\mathbf{1}_2 \cdot \text{CB}[8]_2$), respectively.

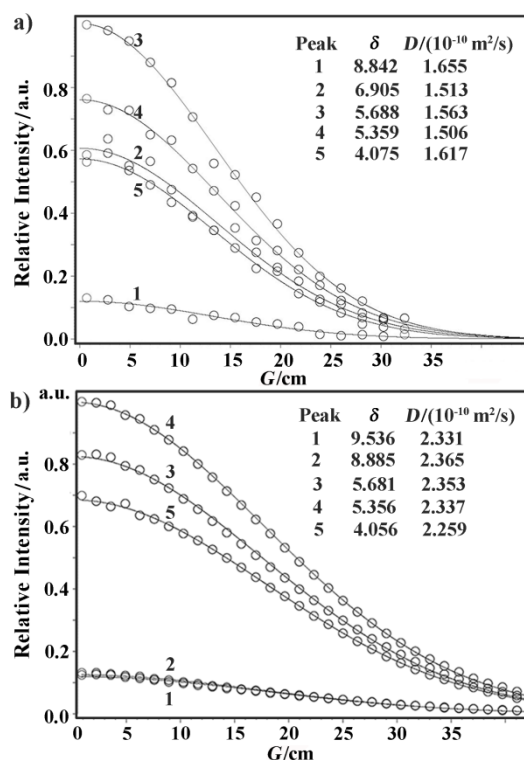


Figure 4 DOSY spectra recorded (600 MHz, D_2O , 298 K) for (a) $\mathbf{1}_2 \cdot \text{CB}[8]_2$ and (b) $\mathbf{1} \cdot \text{CB}[7]_2$. [**1**] = 0.5 mmol/L.

To explore the photophysical properties of **1** and CB[7/8] in aqueous solution, UV-vis and fluorescence titration experiments were performed. First, the UV-vis spectrum of **1** displayed two significant absorption bands centered approximately at 260 and 330 nm (Figure 5a), which are assigned to viologen unit in the middle and naphthalene rings contained in **1**. Under the addition of 1.0 equiv. of CB[8] into the aqueous solution of **1**, a remarkable red shift ($\Delta\lambda = 37 \text{ nm}$) of the peak around 330 nm and one shoulder at 464 nm were observed, ascribing to the charge transfer (CT) process between host and guest. A similar situation also occurs in the UV-vis titration experiment of $\mathbf{1} \cdot \text{CB}[7]_2$: the one absorbance maxima was red-shifted ($\Delta\lambda = 13 \text{ nm}$) from 329 nm to 342 nm, and a CT band at around 433 nm came out (Figure S13). Then, fluorescence titration experiments were performed to investigate the fluorescent emission properties of **1** and $\mathbf{1} \cdot \text{CB}[7/8]$ complexes. With constantly adding CB[8] in an extremely dilute solution of **1** in water, the characteristic of the dual emission was observed, which indicated that the luminescence property originated from the intermolecular interactions (Figures 5b–c): The intensity of

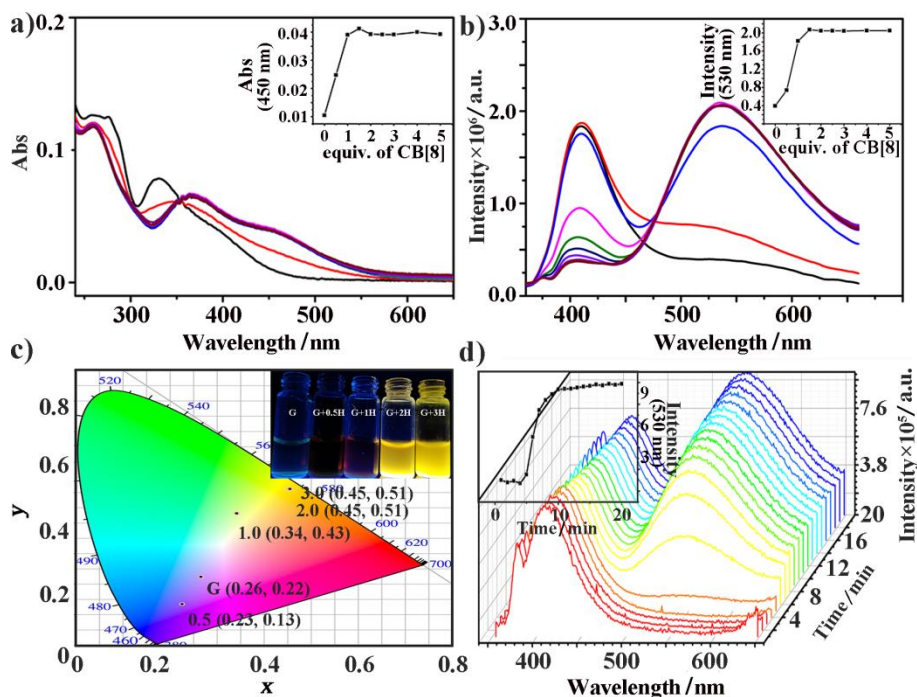


Figure 5 UV-vis absorption (a) and Fluorescence spectra (b) of **1** (10×10^{-6} mol/L) in water upon addition of CB[8]. The inset shows a plot of absorbance intensity at 450 nm and fluorescence intensity at 530 nm versus CB[8] concentration. (c) 1931 CIE chromaticity coordinate changes of **1** ($10.0 \mu\text{mol/L}$) in the presence of CB[8] (0, 0.5, 1.0, 2.0, 3.0 equiv.). The inset shows the examples of fluorescence photographs with CIE coordinate (from left to right) of $1_2 \cdot \text{CB}[8]_2$ (1.0 mmol/L) from bluish violet to orange under the ultraviolet lamp. (d) Fluorescence(2D) spectrum recorded of $1_2 \cdot \text{CB}[8]_2$. The insets show a plot of fluorescence intensity varying with time under 530 nm. $\lambda_{\text{ex}} = 340 \text{ nm}$, $E_{\text{x}}/E_{\text{m}}$ slit = 5 nm.

monomer emission of **1** at 409 nm decreased, accompanied by the appearance of a new emission peak at 535 nm with $\Delta\lambda = 126$ nm, indicating the formation of host-guest complexes with dual guests. Both the UV-vis and fluorescence titration experiments of **1** with CB[8] established a 2 : 2 stoichiometry of $1_2 \cdot \text{CB}[8]_2$. Interestingly, 2D time-dependent fluorescence experiment was performed to research the binding process of **1** and CB[8], suggesting the formation of stable host-guest complex needed about 12 min at least (Figure 5d). Similarly, the emission intensity at 409 nm was gradually decreased and a new emission peak at 524 nm appeared by adding CB[7]. However, the intensity of new peak remained stable when adding an excess of CB[7] (2.0 equiv.) (Figure S14), which supports that the formation of supramolecular assembly of $1 \cdot \text{CB}[7]_2$ is 1 : 2 stoichiometry. Comparing the two fluorescent experiments of pseudo[2,2]rotaxane and pseudo[1,2]-rotaxane, we found that these two pseudorotaxanes exhibited large but varying red-shifting. This observation indicated that the assembled models about **1** with the different ratio of CB[7/8] were definitely different. The two molecules array with a face-to-face stacking pattern in CB[8]'s cavity, which enhanced the supramolecular conjugation and electron transfer process. In the contrast, two CB[7] molecules were at the terminal of the guest molecules, the result of this ability of supramolecular conjugation is lower than that of pseudo[2,2]rotaxane, so the red-shift distance is shorter than that of pseudo[2,2]rotaxane. The 1931 CIE chromaticity coordinate changes of **1** in the presence of CB[7/8] are summarized in Figure 5c and Figure S15, respectively. The fluorescent colors of the system of **1** with different ratio of CB[8] were changed from bluish violet to orange. However, with the different ratio of CB[7], the fluorescent colors of the system changed from bluish violet to pale yellow, including a near white-light emission (0.33, 0.37).

In order to further investigate the binding affinity between CB[7/8] and **1**, we chose a tight binding guest, 3,5-dimethyl-1-adamantylamine-HCl (Me_2ADA), to perform a competitive exper-

iment. When 1.0 equiv. of Me_2ADA was added to the solution of $1_2 \cdot \text{CB}[8]_2$, the emission intensity of the complex decreased at 536 nm and the emission intensity of free **1** gradually increased at 406 nm, suggesting that most of the guest is out of the CB[8] cavity. It is because the binding affinity of **1** with CB[8] is weaker than that of Me_2ADA with CB[8] (Figure S16). This result was also confirmed by ^1H NMR titration experiments (Figure S17). When 3.0 equiv. of Me_2ADA was added, most of the guests came out of the CB[8]'s cavity. These experiments indicate a transformation from $1_2 \cdot \text{CB}[8]_2$ to the highly stable $\text{CB}[8] \cdot \text{Me}_2\text{ADA}$ complex.^[23] By contrast to CB[8], we performed ^1H NMR titration of competitive experiment among **1**, Me_2ADA and CB[7] (Figure S18). When 6.0 equiv. Me_2ADA was added, no guest came out of the CB[7] cavity, suggesting that the binding constant of $1 \cdot \text{CB}[7]_2$ is stronger than that of Me_2ADA with CB[7].

To understand the thermodynamic properties of the pseudo[2,2]rotaxane ($1_2 \cdot \text{CB}[8]_2$) and pseudo[1,2]rotaxane ($1 \cdot \text{CB}[7]_2$), the temperature-dependent fluorescence experiments were performed. The emission of free guest increased at 406 nm and the emission of $1_2 \cdot \text{CB}[8]_2$ decreased at 536 nm and the emission of free guest increased at 406 nm when the temperature rose from 278 K to 343 K (Figure 6a), suggesting the gradual dissociation of $1_2 \cdot \text{CB}[8]_2$. In the case of $1 \cdot \text{CB}[7]_2$, the maximum emission showed blue shift from 524 nm to 503 nm under the increment of external temperature. In this process, one of the two CB[7] would separate from the assembly system (Figure S19). Temperature-dependent ^1H NMR and fluorescence experiments showed that pseudo[2,2]rotaxane ($1_2 \cdot \text{CB}[8]_2$) and pseudo[1,2]-rotaxane were not stable and could be destroyed at higher temperature (Figure S20).

The aggregation behavior of $1 \cdot \text{CB}[7/8]$ was also investigated by fluorescence experiments. As seen in Figures 6b and S21, the fluorescence intensity of $1_2 \cdot \text{CB}[8]_2$ at 540 nm increased linearly as the concentration was gradually raised from 2.0 to 28.2 $\mu\text{mol/L}$, and then slowly increased from 28.2 to 100 $\mu\text{mol/L}$, which implies that the critical aggregate concentration (CAC) of $1_2 \cdot \text{CB}[8]_2$ is

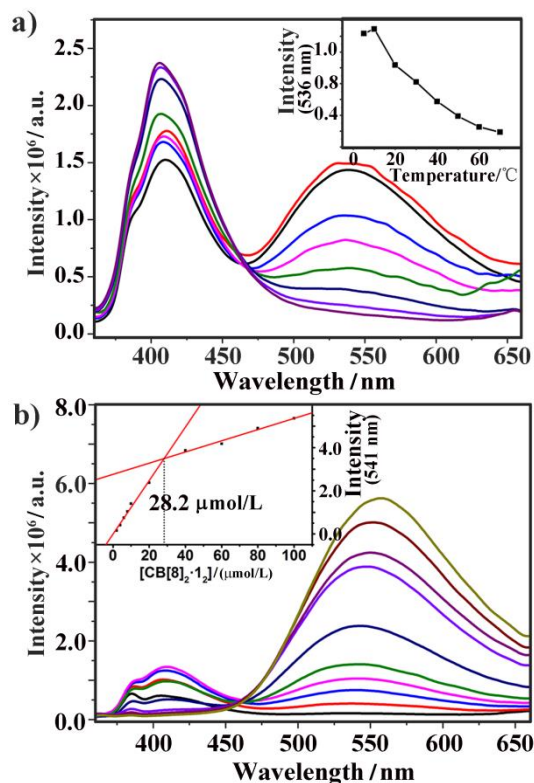


Figure 6 Fluorescence emission spectra: a) the plot of maximum emission intensity at 536 nm of $\text{CB}[8]\cdot\mathbf{1}$ as a function of temperature (5–70 °C). All the measurements were taken using $\text{CB}[8]_2\cdot\mathbf{1}_2$ aqueous solution with unified concentration ($[\text{CB}[8]_2\cdot\mathbf{1}_2] = 10 \mu\text{mol/L}$); b) plot of maximum emission intensity at 541 nm of $\text{CB}[8]\cdot\mathbf{1}$ (2–100 $\mu\text{mol/L}$) in H_2O solution at 298 K. $\lambda_{\text{ex}} = 340 \text{ nm}$, Ex/Em slit = 5 nm.

around 28.2 $\mu\text{mol/L}$. At high concentration, the aggregation or packing of pseudo[2,2]rotaxane $\mathbf{1}_2\cdot\text{CB}[8]_2$ probably enhances the supramolecular conjugation and electron transfer process, leading to an increase in emission and a shift from 540 nm to 556 nm. By contrast, the emission intensity of $\mathbf{1}\cdot\text{CB}[7]_2$ increased and de-

creased linearly with the concentration from 2.0 to 27.4 $\mu\text{mol/L}$ and from 27.4 to 100 $\mu\text{mol/L}$ at 522 nm, respectively, which implies that the CAC of $\mathbf{1}\cdot\text{CB}[7]_2$ is 27.4 $\mu\text{mol/L}$ (Figure S22). Therefore, we concluded that the aggregate state of $\mathbf{1}\cdot\text{CB}[7]_2$ at higher concentration was through non-covalent interactions (*e.g.*, π - π interactions), which could cause aggregation-caused quenching (ACQ) effect.^[24] In addition, quantum yields (Φ) and fluorescence lifetime (τ) of $\mathbf{1}_2\cdot\text{CB}[8]_2$ and $\mathbf{1}\cdot\text{CB}[7]_2$ were measured (Table S1). The quantum yield of $\mathbf{1}_2\cdot\text{CB}[8]_2$ and $\mathbf{1}\cdot\text{CB}[7]_2$ increased to 7.31% and 4.49%, respectively ($\Phi_{\text{F},1} = 2.24\%$). Both $\mathbf{1}_2\cdot\text{CB}[8]_2$ and $\mathbf{1}\cdot\text{CB}[7]_2$ displayed two decay kinetics. Compared with $\mathbf{1}$, the relatively higher τ_{F} was ascribed to the host $\text{CB}[n]$ enhancing the stability of the complexes at the excited state (Figures S23, S24).^[19]

The phenomenon of molecular recognition between different host-guest pairs without mutual interference is called "Self-Sorting".^[25] Scientists manage to utilize self-sorting principle to design and construct a number of complicated systems, such as nanofiber networks,^[26] supramolecular polymers,^[27] supramolecular organic framework^[28] in varieties of applications, such as cell growth,^[29] sensors,^[30] drug solubilization,^[31] and so on. In this paper, a high level of affinity and selectivity between the different guests and $\text{CB}[8]$ is presented in self-sorting process. The self-sorting process, which involves $\mathbf{1}$ and $\mathbf{2}^{13\text{c}}$ as well as cucurbit[8]uril was investigated through the comparison of ^1H NMR spectra (Figures 7 and S25). The ^1H NMR spectrum of guest $\mathbf{1}$ in D_2O was shown in Figure S25a. Upon the addition of one equiv. of $\text{CB}[8]$, the strong host-guest interaction between $\mathbf{1}$ and $\text{CB}[8]$ drove the efficient formation of the pseudo[2,2]rotaxane ($\mathbf{1}_2\cdot\text{CB}[8]_2$) (Figure 7a). In a previous report, $\mathbf{2}$ and $\text{CB}[8]$ were mixed in D_2O in the same molar ratio to form square [5]molecular necklace ($\mathbf{2}\cdot\text{CB}[8]_4$) (Figure 7b). Next, we focused on the self-sorting process of two supramolecular assemblies. As seen in Figure 7c, $\mathbf{1}$ and $\mathbf{2}$ at a molar ratio of 1 : 1 were mixed in one pot, followed by addition of two molar equivalent of $\text{CB}[8]$. Interestingly, after careful analysis, we found that the spectrum showed the same pattern with the simple spectral overlap by the comparisons of different ^1H NMR spectra, which can fully demonstrate that the efficiently and specifically formed $\mathbf{1}_2\cdot\text{CB}[8]_2$ and ($\mathbf{2}\cdot\text{CB}[8]_4$) are the predominant species in this multi-component self-assembly process. It also shows that the two guests and $\text{CB}[8]$ have no interference when they are assembled.

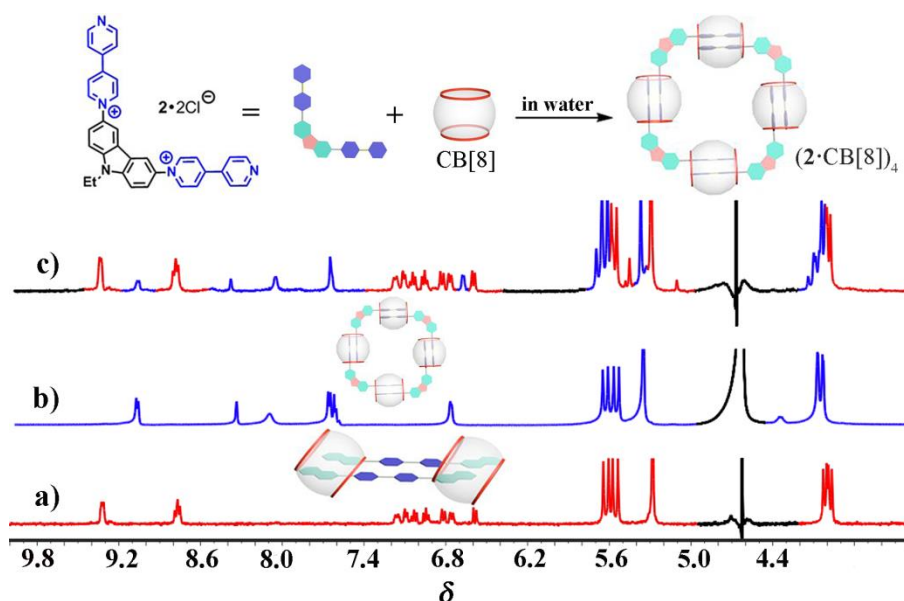


Figure 7 ^1H NMR spectra recorded (400 MHz, 298 K, D_2O) for self-sorting behavior: (a) pseudo[2,2]rotaxane $\mathbf{1}_2\cdot\text{CB}[8]_2$, (b) square molecular neck ($\mathbf{2}\cdot\text{CB}[8]_4$), (c) the mixture of $\mathbf{1}_2\cdot\text{CB}[8]_2$ and ($\mathbf{2}\cdot\text{CB}[8]_4$).

Conclusions

In summary, two kinds of pseudorotaxanes were self-assembled by viologen-naphthalene derivative (**1**), which were successfully synthesized by the Zincke reaction, and CB[7/8] through host-guest interaction. The host-guest recognition of **1** with CB[n] was investigated by ^1H NMR, ESI-MS, COSY, NOESY, DOSY, UV-vis absorption and fluorescence spectra. Based on these two kinds of pseudorotaxanes, we have expanded the definition of [n]rotaxane to offer a precise definition, pseudo[n,m]rotaxanes, to accurately describe the multiaxial pseudorotaxanes. This definition will help people to easily understand the interlocking structures of complicated MIMs. Furthermore, these two pseudorotaxanes exhibit varied photophysical properties, stimuli-responsive behavior triggered by competitive guest, and self-sorting behavior. We expect these kinds of complicated supramolecular assemblies with various supramolecular behaviors can be precisely defined and utilized for potential applications such as molecular switches, sensors, and even information storage.

Experimental

General experimental methods. Starting materials were purchased from commercial suppliers and used without further purification. CB[n] ($n = 7,8$)^[32] was prepared according to the published procedure. Melting points were measured on an XT-4 apparatus in open capillary tubes and are uncorrected. IR spectra were recorded on a JASCO FT/IR 4100 spectrometer and are reported in cm^{-1} . UV-Vis spectra were done on Agilent Cary-100. Fluorescence spectra were recorded on a Horiba Fluorolog-3 spectrometer. Fluorescence decay profiles were recorded on a Flsp920. NMR spectra were measured on a spectrometer operating at 400 MHz for ^1H and 100 MHz for ^{13}C NMR spectra. Mass spectrometry was performed using a JEOL AccuTOF electrospray instrument (ESI). Isothermal titration calorimetry (ITC) was carried out using a VP-ITC (Malvern) at 25 °C, and computer fitting of the data was performed using the VP-ITC analyze software. X-ray crystal diffraction data for **1** were performed on a Bruker D8 Venture photon II diffractometer at low temperature (153 K) with graphite-monochromated Mo K α radiation ($\lambda = 0.71073 \text{ \AA}$).

Synthetic procedures. Compound **1**: **SI3** (892 mg, 1.59 mmol) and **SI4** (500 mg, 3.49 mmol) were mixed in ethanol (10 mL). After being refluxed for 2 d, diethyl ether was added for precipitation. The suspension was poured into a centrifuge tube and centrifuged at 7600 r/min for 5 min at RT. The solid was washed successively with diethyl ether (25 mL), ethyl acetate (25 mL) and acetone (25 mL). Then the solid product was dried under vacuum to give pure **1**·2Cl $^-$ (679 mg, 89%). m.p. 240–241 °C. IR (cm^{-1}): 3104m, 3025m, 1623s, 1587m, 1508m, 1430m, 1329s, 1265m, 815m, 743w. ^1H NMR (400 MHz, D $_2$ O) δ : 9.53 (d, $J = 6.5$ Hz, 4H), 8.85 (d, $J = 6.5$ Hz, 4H), 8.42 (s, 2H), 8.30 (d, $J = 8.8$ Hz, 2H), 8.20–8.10 (m, 4H), 7.89 (dd, $J = 8.8, 2.1$ Hz, 2H), 7.85–7.70 (m, 4H). ^{13}C NMR (100 MHz, DMSO- d_6) δ : 148.9, 146.2, 139.6, 133.5, 132.3, 130.4, 128.9, 128.8, 128.2, 128.1, 126.8, 124.6, 121.7. HRMS: m/z 205.0890 [$[\text{C}_{30}\text{H}_{22}\text{N}_2]^{2+}$, calcd. for $[\text{C}_{30}\text{H}_{22}\text{N}_2]^{2+}$, 205.0886).

Supporting Information

The supporting information for this article is available on the WWW under <https://doi.org/10.1002/cjoc.201800562>.

Acknowledgement

This work was supported by the National Natural Science Foundation of China (Nos. 21771145 and 21472149).

References

- [1] Zhu, Z.; Fahrenbach, A. C.; Li, H.; Barnes, J. C.; Liu, Z.; Dyar, S. M.;

- Zhang, H.; Lei, J.; Carmieli, R.; Sarjeant, A. A.; Stern, C. L.; Wasielewski, M. R.; Stoddart, J. F. Controlling Switching in Bistable [2]Catenanes by Combining Donor–Acceptor and Radical–Radical Interactions. *J. Am. Chem. Soc.* **2012**, *134*, 11709–11720.
- [2] Lee, S.; Lu, W. The Switching of Rotaxane-Based Motors. *Nano. Tech.* **2011**, *22*, 205501.
- [3] Cakmak, Y.; Erbas-Cakmak, S.; Leigh, D. A. Asymmetric Catalysis with a Mechanically Point-Chiral Rotaxane. *J. Am. Chem. Soc.* **2016**, *138*, 1749–1751.
- [4] Li, S.-H.; Zhang, H.-Y.; Xu, X.; Liu, Y. Mechanically Selflocked Chiral Gemini-Catenanes. *Nat. Commun.* **2015**, *6*, 7590.
- [5] Xue, M.; Yang, Y.; Chi, X.; Yan, X.; Huang, F. Development of Pseudorotaxanes and Rotaxanes: from Synthesis to Stimuli-Responsive Motions to Applications. *Chem. Rev.* **2015**, *115*, 7398–7501.
- [6] Schill, G. Catenanes, Rotaxanes, and Knots. In *Organic Chemistry*, Vol. 22, Academic Press, New York, **1971**, p. 192.
- [7] Lagona, J.; Mukhopadhyay, P.; Chakrabarti, S.; Isaacs, L. The Cucurbit[n]uril Family. *Angew. Chem. Int. Ed.* **2005**, *44*, 4844–4870.
- [8] Chen, Z.-H.; Zhou, F.-G.; Zhang, Y.-Q.; Zhu, Q.-J.; Xue, S.-F.; Zhu, T. Crystal Structures of Three Host–Guest Complexes of Methylsubstituted Cucurbit[6]urils and Anthracene Derivatives. *J. Mol. Struct.* **2009**, *930*, 140–146.
- [9] Choi, S.; Park, S. H.; Ziganshina, A. Y.; Ko, Y. H.; Lee, J. W.; Kim, K. A Stable Cis-Stilbene Derivative Encapsulated in Cucurbit[7]uril. *Chem. Commun.* **2003**, *17*, 2176–2177.
- [10] Yang, B.; Yu, S.-B.; Wang, H.; Zhang, D.-W.; Li, Z.-T. 2:2 Complexes from Diphenylpyridiniums and Cucurbit[8]uril: Encapsulation-Promoted Dimerization of Electrostatically Repulsing Pyridiniums. *Chem. Asian J.* **2018**, *13*, 1312–1317.
- [11] Jeon, Y. J.; Bharadwaj, P. K.; Choi, S.; Lee, J. W.; Kim, K. Supramolecular Amphiphiles: Spontaneous Formation of Vesicles Triggered by Formation of a Charge-Transfer Complex in a Host. *Angew. Chem. Int. Ed.* **2002**, *41*, 4474–4476.
- [12] Biedermann, F.; Scherman, O. A. Cucurbit[8]uril Mediated Donor–Acceptor Ternary Complexes: A Model System for Studying Charge-Transfer Interactions. *J. Phys. Chem. B* **2012**, *116*, 2842–2849.
- [13] (a) Pessego, M.; Moreira, J. A.; Costa, A. M. R. D.; Corrochano, P.; Poblete, F. J.; Garcia-Rio, L. Electrostatic Repulsion between Cucurbit[7]urils Can Be Overcome in [3]Pseudorotaxane without Adding Salts. *J. Org. Chem.* **2013**, *78*, 3886–3894; (b) Gromov, S. P.; Vedernikov, A. I.; Kuz'mina, L. G.; Kondratuk, D. V.; Sazonov, S. K.; Strelenko, Y. A.; Alfimov, M. V.; Howard, J. A. K. Photocontrolled Molecular Assembler Based on Cucurbit[8]uril: [2+2]-Autophotocycloaddition of Styryl Dyes in the Solid State and in Water. *Eur. J. Org. Chem.* **2010**, *13*, 2587–2599; (c) Baroncini, M.; Gao, C.; Carboni, V.; Credi, A.; Previtara, E.; Semeraro, M.; Venturi, M.; Silvi, S. Light Control of Stoichiometry and Motion in Pseudorotaxanes Comprising a Cucurbit[7]uril Wheel and an Azobenzene Bipyridinium Axle. *Chem. Eur. J.* **2014**, *20*, 10737–10744; (d) Gamal-Eldin, M. A.; Macartney, D. H. Cucurbit[7]uril Host–Guest Complexes and [2]Pseudorotaxanes with N-methylpiperidinium, N-methylpyrrolidinium, and N-methylmorpholinium Cations in Aqueous Solution. *Org. Biomol. Chem.* **2013**, *11*, 1234–1241; (e) Jiang, W.; Wang, Q.; Linder, I.; Klautzsch, F.; Schalley, C. A. Self-Sorting of Water-Soluble Cucurbituril Pseudorotaxanes. *Chem. Eur. J.* **2011**, *17*, 2344–2348; (f) Zhang, Y.; Zhou, T.-Y.; Zhang, K.-D.; Dai, J.-L.; Zhu, Y.-Y.; Zhao, X. Encapsulation Enhanced Dimerization of a Series of 4-Aryl-NMethylpyridinium Derivatives in Water: New Building Blocks for Self Assembly in Aqueous Media. *Chem. Asian J.* **2014**, *9*, 1530–1534; (g) Liu, Y.; Shi, K.; Ma, D. Water-Soluble Pillar[n]arene Mediated Supramolecular Self-Assembly: Multi-Dimensional Morphology Controlled by Host Size. *Chem. Asian J.* **2018**, DOI: 10.1002/asia.201801705; (h) Wei, P.; Yan, X.; Huang, F. Reversible Formation of a Poly[3]rotaxane Based on Photo Dimerization of an Anthracene-Capped [3]Rotaxane. *Chem. Commun.* **2014**, *50*, 14105–14108.
- [14] (a) Whang, D.; Kim, K. Polycatenated Two-Dimensional Polyrotaxane Net. *J. Am. Chem. Soc.* **1997**, *119*, 451–452; (b) Lee, E.; Kim, J.; Heo, J.;

- Whang, D.; Kim, K. A Two-Dimensional Polyrotaxane with Large Cavities and Channels: A Novel Approach to Metal-Organic Open-Frameworks by Using Supramolecular Building Blocks. *Angew. Chem. Int. Ed.* **2001**, *40*, 399–402.
- [15] (a) Samanta, S. K.; Brady, K. G.; Isaacs, L. Self-Assembly of Cucurbit[7]uril Based Triangular [4]molecular Necklaces and Their Fluorescence Properties. *Chem. Commun.* **2017**, *53*, 2756–2759; (b) Whang, D.; Park, K.-M.; Heo, J.; Ashton, P.; Kim, K. Molecular Necklace: Quantitative Self-Assembly of a Cyclic Oligorotaxane from Nine Molecules. *J. Am. Chem. Soc.* **1998**, *120*, 4899–4900; (c) Li, J.; Yu, Y.; Luo, L.; Li, Y.; Wang, P.; Cao, L.; Wu, B. Square [5]molecular Necklace Formed from Cucurbit[8]uril and Carbazole Derivative. *Tetrahedron Lett.* **2016**, *57*, 2306–2310.
- [16] (a) Lee, E.; Heo, J.; Kim, K. A Three-Dimensional Polyrotaxane Network. *Angew. Chem. Int. Ed.* **2000**, *39*, 2699–2701; (b) Fan, Z.-F.; Xiao, X.; Zhang, Y.-Q.; Xue, S.-F.; Zhu, Q.-J.; Tao, Z.; Wei, G. A Three Dimensional Framework Induced by π - π Stacking of 2,2'-(Alkylene-1,6-diyl)diisoquinolinium from Q[6]-Based Pseudorotaxane. *J. Incl. Phenom. Macrocycl. Chem.* **2011**, *71*, 577–581; (c) Sun, X.; Li, B.; Cao, J.; Chen, J.; Wang, N.; Wan, D.; Zhang, H.; Zhou, X. Pseudopolyrotaxanes of Cucurbit[6]uril: A Three-Dimensional Network Self-assembled by $\text{ClO}_4^-(\text{H}_2\text{O})_2$ Water Clusters. *Chin. J. Chem.* **2012**, *30*, 941–946; (d) Zhang, C.-C.; Zhang, Y.-M.; Liu, Y. Photocontrolled Reversible Conversion of a Lamellar Supramolecular Assembly Based on Cucurbiturils and a Naphthalenediimide Derivative. *Chem. Commun.* **2018**, *54*, 13591–13594.
- [17] Chen, X.-M.; Chen, Y.; Yu, Q.; Gu, B.-H.; Liu, Y. Supramolecular Assemblies with Near-Infrared Emission Mediated in Two Stages by Cucurbituril and Amphiphilic Calixarene for Lysosome-Targeted Cell Imaging. *Angew. Chem. Int. Ed.* **2018**, *57*, 12519–12523.
- [18] (a) Zhang, K.-D.; Tian, J.; Hanifi, D.; Zhang, Y.; Sue, A. C.-H.; Zhou, T.-Y.; Zhang, L.; Zhao, X.; Liu, Y.; Li, Z.-T. Toward a Single-Layer Two-Dimensional Honeycomb Supramolecular Organic Framework in Water. *J. Am. Chem. Soc.* **2013**, *135*, 17913–17918; (b) Li, Y.; Dong, Y.; Miao, X.; Ren, Y.; Zhang, B.; Wang, P.; Yu, Y.; Li, B.; Isaacs, L.; Cao, L. Shape-Controllable and Fluorescent Supramolecular Organic Frameworks Through Aqueous Host-Guest Complexation. *Angew. Chem. Int. Ed.* **2018**, *57*, 729–733.
- [19] Li, S.-H.; Xu, X.; Zhou, Y.; Zhao, Q.; Liu, Y. Reversibly Tunable White-Light Emissions of Styrylpyridiniums with Cucurbiturils in Aqueous Solution. *Org. Lett.* **2017**, *19*, 6650–6653.
- [20] (a) Kotturi, K.; Masson, E. Directional Self-Sorting with Cucurbit[8]uril Controlled by Allosteric π - π and Metal-Metal Interactions. *Chem. Eur. J.* **2018**, *24*, 8670–8678; (b) Liu, Y.; Yang, H.; Wang, Z.; Zhang, X. Cucurbit[8]uril-Based Supramolecular Polymers. *Chem. Asian J.* **2013**, *8*, 1626–1632; (c) Chakrabarti, S.; Isaacs, L. Cucurbit[8]uril Controls the Folding of Cationic Diaryl Ureas in Water. *Supramol. Chem.* **2008**, *20*, 191–199; (d) Ko, Y. H.; Kim, K.; Kim, E.; Kim, K. Exclusive Formation of 1:1 and 2:2 Complexes between Cucurbit[8]uril and Electron Donor-Acceptor Molecules Induced by Host-stabilized Charge-transfer Interactions. *Supramol. Chem.* **2007**, *19*, 287–293; (e) Barrio, J. D.; Ryan, S. T. J.; Jambrina, P. G.; Rosta, E.; Scherman, O. A. Light-Regulated Molecular Trafficking in a Synthetic Water-Soluble Host. *J. Am. Chem. Soc.* **2016**, *138*, 5745–5748; (f) Liu, Y.; Yu, Y.; Gao, J.; Wang, Z.; Zhang, X. Water-Soluble Supramolecular Polymerization Driven by Multiple Host-Stabilized Charge-Transfer Interactions. *Angew. Chem. Int. Ed.* **2010**, *49*, 6576–6579.
- [21] Wu, G.; Olesinska, M.; Wu, Y.; Matak-Vinkovic, D.; Scherman, O. A. Mining 2:2 Complexes from 1:1 Stoichiometry: Formation of Cucurbit[8]uril-Diaryliologen Quaternary Complexes Favored by Electron-Donating Substituents. *J. Am. Chem. Soc.* **2017**, *139*, 3202–3208.
- [22] Yu, Y.; Li, Y.; Wang, X.; Nian, H.; Wang, L.; Li, J.; Zhao, Y.; Yang, X.; Liu, S.; Cao, L. Cucurbit[10]uril-Based [2]Rotaxane: Preparation and Supramolecular Assembly-Induced Fluorescence Enhancement. *J. Org. Chem.* **2017**, *82*, 5590–5596.
- [23] Barrow, S. J.; Kasera, S.; Rowland, M. J.; Barrio, J. D.; Scherman, O. A. Cucurbituril-Based Molecular Recognition. *Chem. Rev.* **2015**, *115*, 12320–12406.
- [24] Hong, Y.; Lam, J. W. Y.; Tang, B. Aggregation-induced Emission. *Chem. Soc. Rev.* **2011**, *40*, 5361–5388.
- [25] Mukhopadhyay, P.; Wu, A.; Isaacs, L. Social Self-Sorting in Aqueous Solution. *J. Org. Chem.* **2004**, *69*, 6157–6164.
- [26] Shigemitsu, H.; Fujisaku, T.; Tanaka, W.; Kubota, R.; Minami, S.; Hamachi, K.; Hamachi, I. An Adaptive Supramolecular Hydrogel Comprising Self-Sorting Double Nanofibre Networks. *Nat. Nanotech.* **2018**, *13*, 165–172.
- [27] Huang, Z.; Qin, B.; Chen, L.; Xu, J.-F.; Faul, C. F. J.; Zhang, X. Supramolecular Polymerization from Controllable Fabrication to Living Polymerization. *Macromol. Rapid Commun.* **2017**, *38*, 1700312.
- [28] Pfeffermann, M.; Dong, R.; Graf, R.; Zajackowski, W.; Gorelik, T.; Pisula, W.; Narita, A.; Müllen, K.; Feng, X. Free-Standing Monolayer Two-Dimensional Supramolecular Organic Framework with Good Internal Order. *J. Am. Chem. Soc.* **2015**, *137*, 14525–14532.
- [29] Vieira, V. M. P.; Lima, A. C.; Jong, M. D.; Smith, D. K. Commercially Relevant Orthogonal Multi-Component Supramolecular Hydrogels for Programmed Cell Growth. *Chem. Eur. J.* **2018**, *24*, 15112–15118.
- [30] Shang, X.; Song, I.; Jung, G. Y.; Choi, W.; Ohtsu, H.; Lee, J. H.; Koo, J. Y.; Liu, B.; Ahn, J.; Kawano, M.; Kwak, S. K.; Oh, J. H. Chiral Self-Sorted Multifunctional Supramolecular Biocoordination Polymers and Their Applications in Sensors. *Nat. Commun.* **2018**, *9*, 3933.
- [31] Ganapati, S.; Isaacs, L. Acyclic Cucurbit[n]uril-Type Receptors: Preparation, Molecular Recognition Properties and Biological Applications. *Isr. J. Chem.* **2018**, *58*, 250–263.
- [32] Kim, J.; Jung, I.-S.; Kim, S.-Y.; Lee, E.; Kang, J.-K.; Sakamoto, S.; Yamaguchi, K.; Kim, K. New Cucurbituril Homologues: Syntheses, Isolation, Characterization, and X-ray Crystal Structures of Cucurbit[n]uril ($n = 5, 7$, and 8). *J. Am. Chem. Soc.* **2000**, *122*, 540–541.

Manuscript received: December 12, 2018

Manuscript revised: January 9, 2019

Manuscript accepted: January 11, 2019

Accepted manuscript online: January 24, 2019

Version of record online: February 6, 2019